SUPPORTING INFORMATION

Nanopattern matrix. A nanopattern testmatrix was designed in order to find a the optimum dimensions of the six-dot lines for the AuNPs assembly; the center-to-center pitch distance and the diameter of the dots were varied in x- and y-direction as illustrated in Figure SI-1A. AFM mircrographs shown in Figure SI-1B depict the testmatrix with rescessed features.

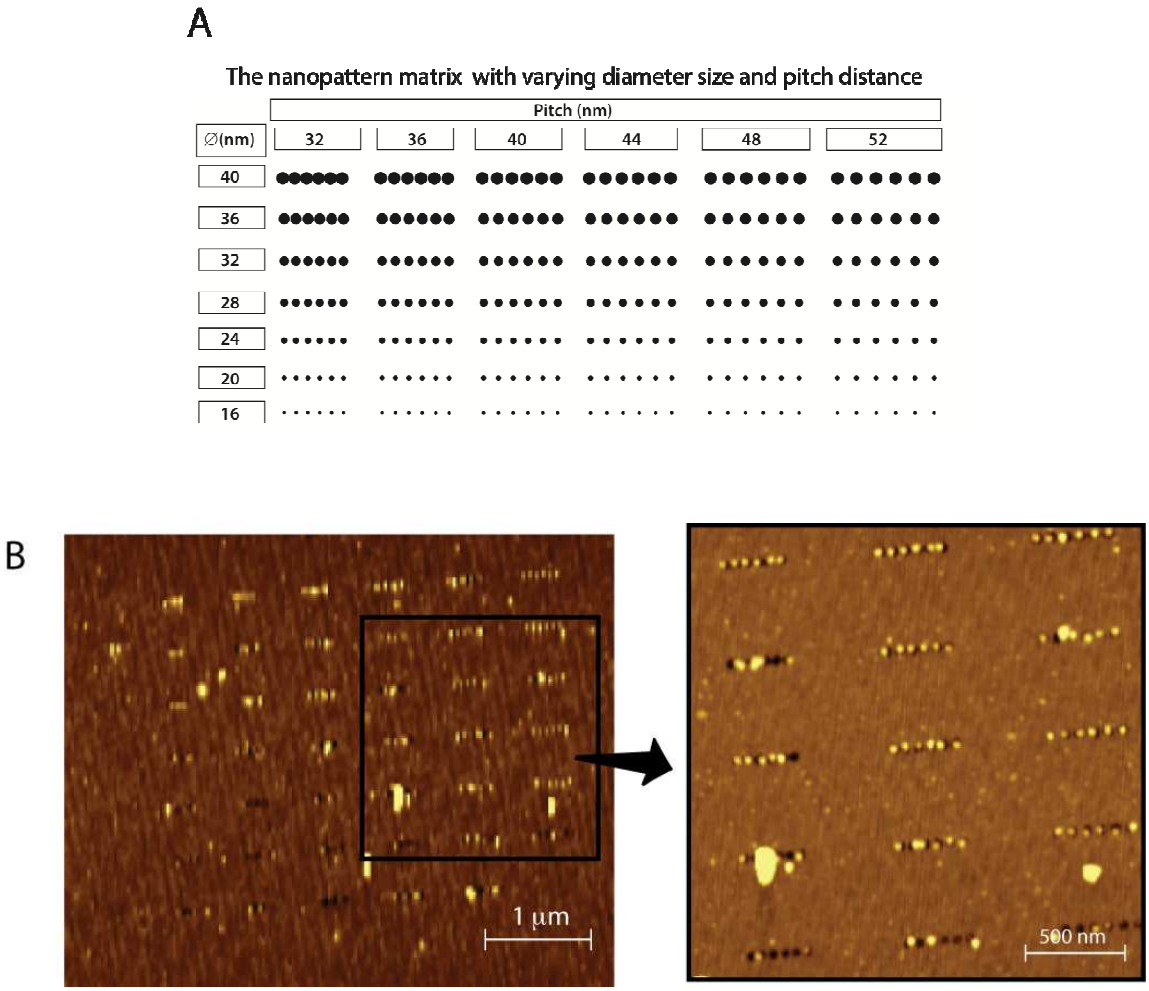

Figure S1. The testmatrix designed to find the optimum dimensions of the templating nanostructures: (A) the center-to-center pitch distance varied in x-direction and the dot diameter size varied in y direction, (B) AFM micrographs of the testmatrix.

It was observed that for six-dot lines comprising of holes with diameter size smaller than 28 nm and center-to-center pitch size smaller than 48 nm, gold did not deposite into the holes.

Typical AFM-micrographs of the testmatrix following the AuNP self-assembly process are shown in Figure SI-2.

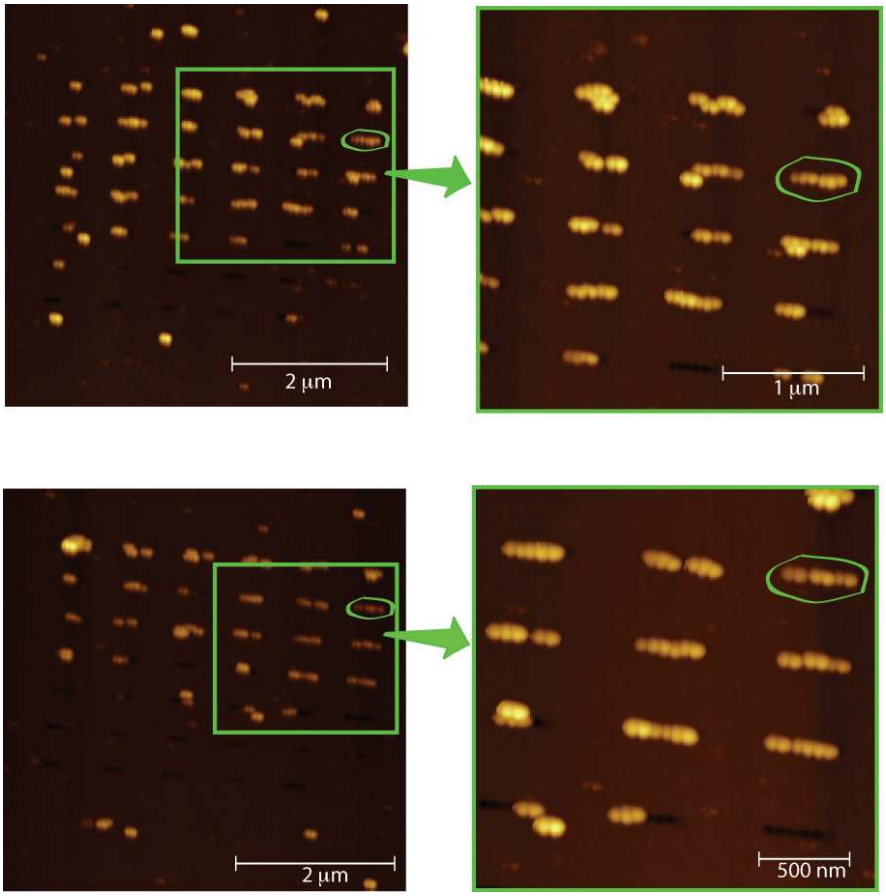

Figure SI-2. Typical AFM micrographs of two testmatrices following the AuNP self-assembly process; the underlying six-dot lines with the selected geometry are encircled.

The AuNPs were observed to more effectively reproduce the templating nanostructure on the six-dot lines with 36 nm dot diameters and 52 nm center-to-center pitch distance and was therefore fabricated over a large area for the statistical analysis (examples shown in Figure SI-2).

Effect of hybridization conditions on assembly efficiency for *sub-A*. Changing the hybridisation conditions when assembling AuNPs onto *sub-A* slightly modified the configuration of the immobilised assemblies. When lowering the concentration of the DNA solution during the surface crafting step and DNA capped concentration of AuNP-DNA conjugate solution during the particle assembly step, more of the 6-dot-lines in the nanopattern only had particles adsorbed to one side of the line (Figure SI-1). The sample displayed in the AFM micrograph in Figure SI-3A, was functionalized in a 10 μM DNA (surface and linker) solution and 3 nM AuNP-DNA conjugate solution, whereas the sample depicted in Figure SI-3B was functionalised in a 0.1 μM DNA (surface and linker), and 0.6 nM AuNP-DNA conjugate solution.

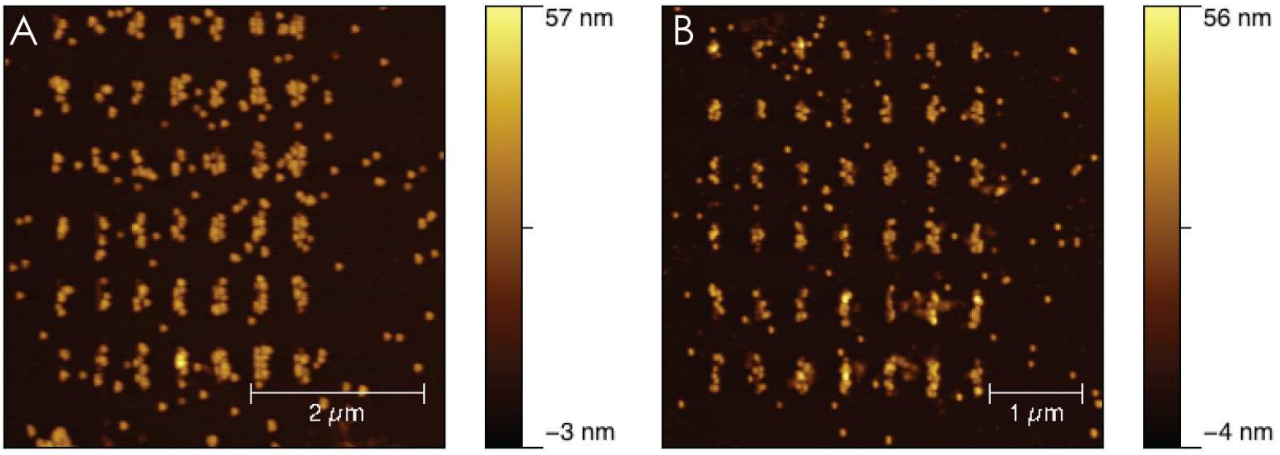

Figure SI-3. AFM micrographs of sub-A's following the AuNP self-assembly process, altering the concentrations of the solutions of surface and linker DNA and of the AuNP-DNA conjugates: (A) functionlalised in a 10 μM DNA (surface and linker) and 3 nM AuNP-DNA conjugate solution, and (B) functionalized in a 0.1 μM DNA (surface and linker), and 0.6 nM AuNP-DNA conjugate solution.

Negative controls. When the AuNPs were self-assembled onto the templating nanostructures with no linker DNA, no immobilzation was observed. Figure SI-4 show AFM micrographs following the self-assembly process: (A) sub-A, with positive features, and (B) sub-B with negative features.

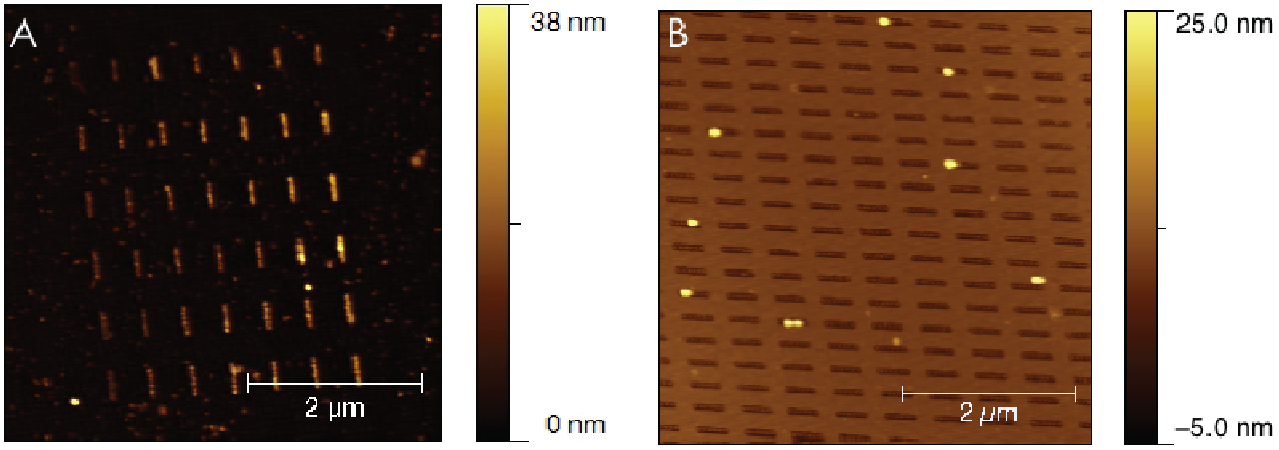

Figure SI-4. AFM micrographs of (A) sub-A and (B) sub-B when self-assembling AuNP-DNA conjugates onto the templating nanostructures with no linker DNA.

Calculation of hybridization efficiency onto *sub-B*. The hybridization efficiency onto *sub-B* was calculated by assessing the number of particles that assembled onto each six-dot line, of 922 assessed, as well as the configuration the AuNPs assembled into. An SEM micrograph of the substrate that served as base for the statistical analysis is shown in Figure SI-5.

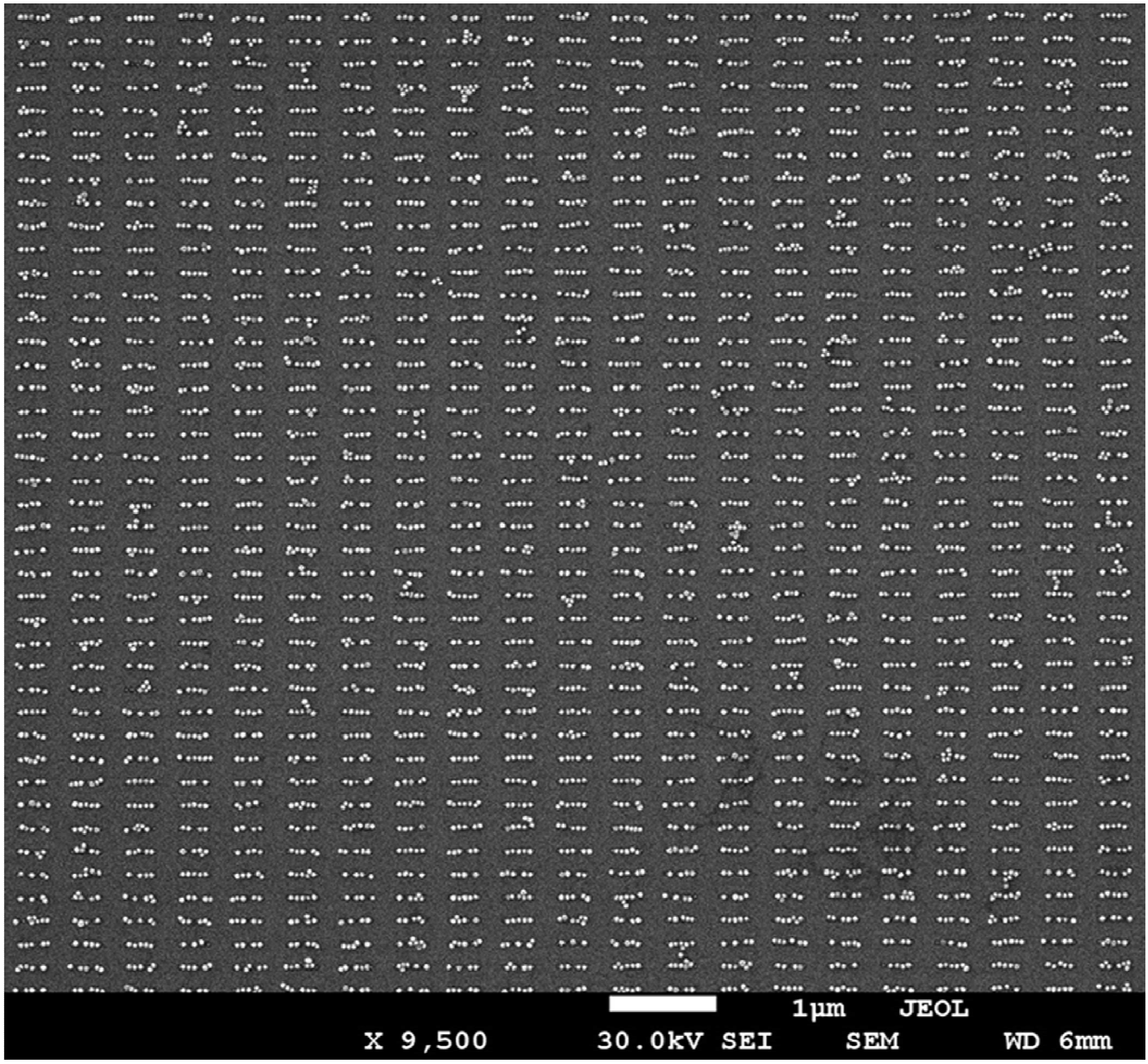

Figure SI-5. A typical SEM micrograph of sub-B following the AuNP self-assembly proces.

Each six-dot line was assumed to have six available adsorption sites. Only the particles that were adsorbed onto the six-dot line were accounted for, *i.e.* a six-dot line with 5 AuNPs, where one of the particles adsorb onto the side of another particle, was considered to have 4 AuNPs on the six-dot line and therefore occupy 4 adsorption sites, leaving two sites un-occupied. Table SI-1 show the assessment.

Table SI-1. The number of vacancies observed following the AuNP self-assembly process onto *sub-B*.

# AuNP in assembly	Configuration group	# of vacancies in assembly	Total # of assemblies	Total # of vacancies	% of vacancies of total # of adsorption sites
3	1 & 2	3	10	30	0.54

4	1 & 2	2	209	418	7.6
4	3	3	7	21	0.38
5	1 & 2	1	338	338	6.1
5	3	2	120	240	4.3
6	3	1	106	106	1.9
TOTAL	**All**	**-**	**922**	**1153**	**20.8**

Of the total number of available adsorption sites, 20.8% were un-occupied, yielding a 79.2% hybridization efficiency.

Effect of hybridization condition on hybridization efficiency. The effect of hybridization condition was investigated. Figure SI-4 shows AFM micrographs of the nanopattern arrays following the self-assembly process, where the linker DNA and AuNP hybridization steps were altered. For the substrate depicted in Figure SI-4A the DNA linker and AuNPs were co-adsorbed, the linker DNA and AuNP-DNA conjugate solution were mixed in a round bottom flask and the substrate immersed. The flask was placed in a 64ºC water bath, the heat was turned off and the temperature of the water allowed to slowly reach RT. For the substrate presented in Figure SI-6B the the hybridization of DNA linker took place in a temperature controlled hybridization chamber (TC), initially the temperature was 64ºC and decreased to 25ºC over 10 min, where it was maintained for the remaining hybridization time. The AuNP hybridization took place in a round bottom flask that was placed in a 42^{o}C water bath, where the temperature of the water was allowed to slowly reach RT.

Figure SI-6. SEM micrographs showing the assembly configuration when assembling onto sub-B's under different DNA and AuNP hybridisation conditions: (A) linker DNA and the AuNPs were co-hybridized, in a water bath left to slowly reach RT, and for (B) the hybridization of the DNA linker was conducted in a temperature controlled hybridization chamber (HC), commencing at 64ºC and decreased to 25ºC over 10 min, and the AuNP hybridization was conducted in a 42ºC water bath that was left to slowly reach RT.

In the micrographs the effect of the hybridization conditions on the configuration the assemblies is clearly visulized. It does not however appear to have a profund effect on the hybridization efficiency. The co-adsorption of linker DNA and AuNPs appeared to yield a more dispersed ranged of assemblies and more particle agglomerates and side-on adsorption of AuNPs.

Effect of etch time on hybridization efficiency. The effect the etching time had on the configuration of the self-assembled AuNPs was also investigated. Figure SI-5 shows SEM micrographs of nanopatterned, substrates that had been etched for different periods of time, following the AuNP self-assembly process.

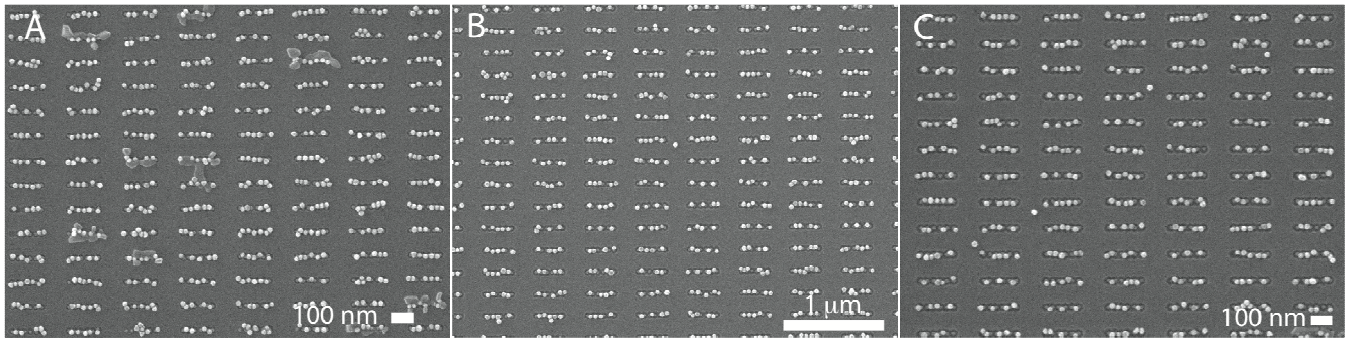

Figure SI-7. SEM micrographs displaying the AuNP hybridization efficiency onto sub-B's etched for different periods of time: (A) 15 s etching, (B) 17 s etching and (C) 20 s etching.

The substrate etched for 15 s (Figure SI-7) had the highest hybridisation efficiency (80%), however, also the highest occurrence of side on adsorption (4.1%). When increasing the depth of the nanopattern holes, the side-on adsorption was reduced to 3 and 2% for the substrates etched for 17 and 20 s, respectively; although, at the expense of the over all hybridisation efficiency (to 73% in in both cases). It appeared as if the holes were too deep, making it difficult for the particle DNA to interact with the surface confined linker DNA. The decrease in side-on adsorption is probably an outcome of the same effect: as the linker DNA does not stretch far enough for its sticky-end to be exposed far beyond the templating nanostructure. Another issue was the increased radii of the array dots, which lead to a higher occurrence of crooked and zig zagged lines (comparing (A) to (B) and (C) in Figure SI-7) The increase in the dot diameter was due to the etchant, ammonium bifluoride, which was an isotropic etchant (etches in all directions). In order to etch a deeper hole, without increasing the diameter, an anisotropic etchant needs to be employed, *e.g.* reactive ion etching.